Computer-aided diagnosis of emphysema in COPD patients: neural-network-based analysis of lung shape in digital chest radiographs.

Available online at www.sciencedirect.com
ScienceDirect
Medical Engineering & Physics 29 (2007) 76–86
Medical Engineering & Physics
www.elsevier.com/locate/medengphy

Computer-aided diagnosis of emphysema in COPD patients: Neural-network-based analysis of lung shape in digital chest radiographs

Giuseppe Coppini *, Massimo Miniati, Marco Paterni, Simonetta Monti, Ezio Maria Ferdeghini

Institute of Clinical Physiology, National Research Council, Pisa, Italy

Received 8 September 2005; received in revised form 27 January 2006; accepted 1 February 2006

Abstract

Several abnormalities of the shape of lung fields (depression and flattening of the diaphragmatic contours, increased retrosternal space) are indicative of emphysema and can be accurately imaged by digital chest radiography. In this work, we aimed at developing computational descriptors of the shape of the lung silhouette able to capture the alterations associated with emphysema. We analyzed two-sided digital chest radiographs from a sample of 160 patients with chronic obstructive pulmonary disease (COPD), 60 of which were affected by emphysema, and from 160 subjects with normal lung function. Two different description schemes were considered: a first one based on lung-silhouette curvature features, and a second one based on a minimal-polyline approximation of the lung shape. Both descriptors were employed to recognize alterations of the lung shape using classifiers based on multilayer neural networks of the feed-forward type.

Results indicate that pulmonary emphysema can be reliably diagnosed or excluded by using digital chest radiographs and a proper computational aid. Two-sided chest radiographs provide more accurate discrimination than single-view analysis. The minimal-polyline approximation provided significantly better results than those obtained from curvature-based features. Emphysema was detected, in the entire dataset, with an accuracy of about 90% (sensitivity 88%, specificity 90%) by using the minimal-polyline approximation.

Keywords: COPD; Emphysema; Digital radiography; Shape analysis; Neural networks

1. Introduction

Pulmonary emphysema is defined as an abnormal, permanent enlargement of the airspaces distal to the terminal bronchioles with destruction of their walls [1]. Since emphysema is a structural pulmonary abnormality, its recognition is based on tests that reflect lung structure rather than function. High-resolution computed tomography (HRCT) is currently the most accurate imaging technique for diagnosing emphysema in vivo [2]. Extensive use of this technique seems, however, unwarranted due to the high cost and substantial radiation burden to the patient. On the other hand, conventional chest radiography is far less expensive than HRCT and entails a much lower effective radiation dose.

Radiographic abnormalities suggestive of emphysema are, in general, of two types: those related to hyperinflation (depression and flattening of the diaphragmatic contours, increased retrosternal space), and those related to the distribution of destructive lesions and concomitant changes in the vascular pattern [3]. Recognition of the latter changes is difficult and often results in large interobserver variability [4]. Conversely, signs of lung hyperinflation are more easily detectable even by less experienced physicians [4]. Correct recognition of emphysema on chest radiograph depends not only on the physician's expertise but also on the film quality. For example, an overexposed film makes the evaluation of vascular abnormalities nearly impossible. On the other hand, a grossly underexposed film may preclude the evaluation of

* Corresponding author. Tel.: +39 0503153480; fax: +39 0503152166.
E-mail address: coppini@ifc.cnr.it (G. Coppini).

1350-4533/$ – see front matter © 2006 IPEM. Published by Elsevier Ltd. All rights reserved.
doi:10.1016/j.medengphy.2006.02.001

the diaphragmatic contours and of the width of the retrosternal space.

Most of the above technical limitations are overcome by digital chest radiography, an imaging modality that is now available in most hospitals [5]. This technique features excellent density resolution and enhanced dynamic range, and offers the opportunity of image processing and quantitative analysis not available in conventional film-based technology [5]. The relevance of quantitative analysis in digital chest radiography is enlightened by the recent advances of Computer Aided Diagnosis (CAD) systems in different clinical tasks [6].

The present study was aimed at developing computational descriptors of the shape of the lung silhouette able to capture the alterations associated with emphysema. To this end, we analyzed two-sided digital chest radiographs from a large sample of patients with chronic obstructive pulmonary disease (COPD) and from an equally sized sample of subjects with normal lung function. Two different description schemes were considered: a first one that was based on lung-silhouette curvature, and a second one relied on a minimal-polyline approximation. Both descriptors were employed to recognize alterations of lung shape related to emphysema using neural-networks-based classifiers.

2. Methods

2.1. Sample

The study sample included 320 subjects of whom 160 had a firm clinical diagnosis of stable COPD and 160 were age- and sex-matched smokers, or ex-smokers, with normal lung function tests. The sample was part of a larger cohort enrolled in a case-control study that was aimed at assessing genetic susceptibility to the development of COPD [7].

2.2. Chest radiography

Posteroanterior and lateral digital chest radiographs (Thorax 2000, IMIX, Finland) were obtained at a standard 2-m focus-to-detector distance with the patients upright, holding their breath at full inspiration. Each radiograph was 2000×2000 pixels (198 μm per pixel), with a dynamic range of 12 bits. Images were obtained by the acquisition equipment in standard operational conditions, and no further post-processing was applied.

Chest radiographs were examined by two independent chest physicians for the presence or absence of emphysema. In evaluating emphysema, four radiographic criteria were used that were originally introduced by Sutinen et al. [3]. The radiographic criteria are described in Table 1. According to Sutinen et al., the diagnosis of emphysema is made when the chest radiographs reveal any two or more of these criteria [3]. In the original report [3], emphysema was correctly identified in *ante-mortem* chest films of 82% of the patients who had autopsy proven emphysema. By contrast, all of the chest radiographs corresponding to the patients with structurally normal lungs were rated as normal. In that study, the overall accuracy of chest radiography in diagnosing or excluding emphysema was 90% [3].

According to the above criteria, 60 of the 160 COPD patients were consistently rated by the two readers as having emphysema. All the subjects with normal lung function tests had no evidence of emphysema on chest radiographs.

2.3. Description of lung shape

Morphological alterations of the lung silhouette related to hyperinflation (diaphragm flattening, blunting of costophrenic angles, abnormal retrosternal space) are the most prominent radiographic abnormalities that can be observed in patients with emphysema. It is worth noting that the decision rule for radiological diagnosis of emphysema actually implies the presence of at least one sign of lung shape alteration.

2.3.1. Lung silhouette

In both the posteroanterior and lateral views an expert physician (not aware of the patient's diagnosis) interactively traced the lung field boundaries, according to the following procedure. The chest radiographs had the identification data removed, and were randomly assigned. The observer located a small set of knot points (typically about 25 knots).

Table 1
Criteria for radiographic diagnosis of emphysema

Signs in the posteroanterior chest radiograph
Depression and flattening of the diaphragm with blunting of costophrenic angles: The actual level of the diaphragm is not as significant as the contour. The body build of the subject should also be considered. In a short, stocky subject, this sign might be positive even if the diaphragm were at the level of the 10th rib posteriorly.
Irregular radiolucency of the lung fields: This manifestation is the result of the irregularity in distribution of the emphysematous tissue destruction.
Signs in the lateral chest radiograph
Abnormal retrosternal space: This is defined as a space showing increased radiolucency and measuring 2.5 cm or more from the sternum to the most anterior margin of the ascending aorta.
Flattening or even concavity of diaphragmatic contours: A useful index of this change is the presence of a 90° or larger sternodiaphragmatic angle. In most patients with emphysema, this junction is more readily seen than in subjects with normal chests.

Fig. 1. Posteroanterior (left) and lateral (right) radiographs from a normal subject.

Afterwards, using a basis of cubic splines, the contour of the lung areas was drawn. Examples are given in Figs. 1 and 2 that refer to chest radiographs from a normal subject and a patient with emphysema, respectively. The overall time required to delineate the lung boundary in a pair of chest radiographs is, on the average, 3 min. It must be pointed out that the needed set of knots is unambiguously identifiable in the imaged anatomy. In particular, we observed that fluctuations less than five pixels might alter knot positioning: a range of fluctuations that does not affect the descriptors of the lung shape adopted in this work.

The analysis of the mediastinal contours is not relevant for emphysema characterization (see Table 1). Therefore, to our aims, in the posteroanterior view, we merged the pulmonary contours of both the lungs not taking the mediastinum borders into account, as shown in Fig. 3 (left). In the lateral view, the contour traced by the physician was directly utilized (see the right panel of Fig. 3).

2.3.1.1. Curvature-based description. The curvature of a plane curve is a commonly used descriptor of bidimensional shapes. Let $\mathbf{r}(s) = (x(s), y(s))$ be the parametric equation of the boundary, where s is the related curvilinear abscissa. By virtue of the Frenet-Serret theorem, the curvature $\kappa(s)$ identifies the shape of the curve $\mathbf{r}(s)$, apart from a rigid motion. In particular, $\kappa(s)$ is well suited to locate different feature points: as an example, a steep change of $\kappa(s)$ is usually related to an abrupt bending of the curve. Similarly, a peak in $\kappa(s)$ is commonly due to a sudden change of the curve tangent and signals the presence of a cusp-like angular feature.

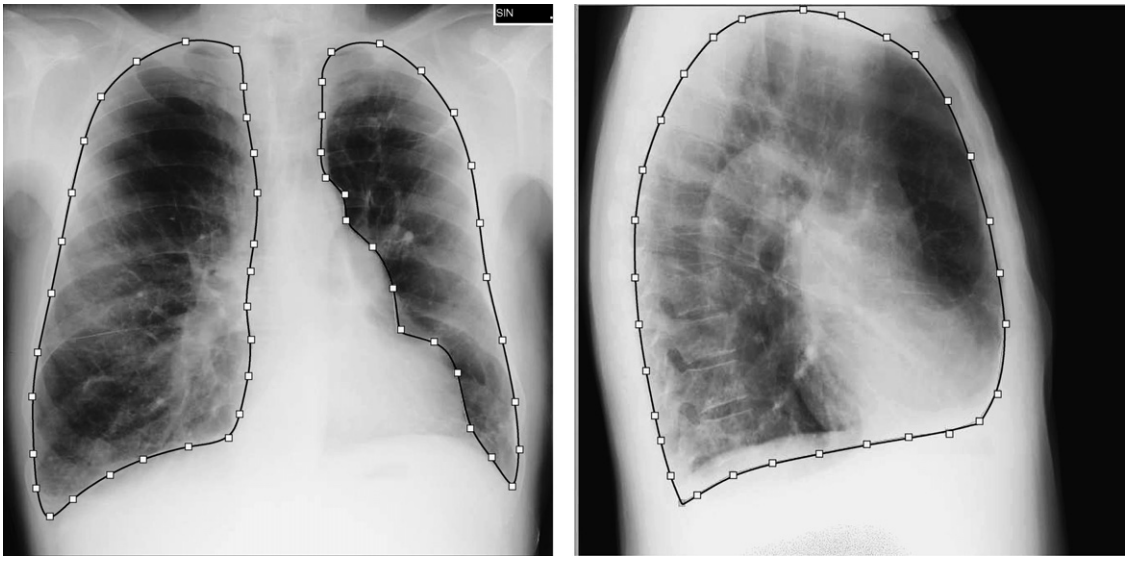

Fig. 2. Posteroanterior (left) and lateral (right) radiographs from a subject with emphysema.

Fig. 3. The lung zone silhouette in posteroanterior and lateral projections (normal subject).

We utilized the curvature of lung silhouette both to recognize landmarks points useful to segment the silhouette into anatomically meaningful sections, and to describe the shape of each segment. To compute $\kappa(s)$ we utilized the equation:

$$\mathbf{r}(s) = \frac{x'(s)y''(s) - x''(s)y'(s)}{(x'(s)^2 + y'(s)^2)^{3/2}}$$

where $(x'(s), y'(s))$, and $(x''(s), y''(s))$ are the first and second derivative of $(x(s), y(s))$ with respect to s, respectively. They were estimated through the convolution of $(x(s), y(s))$ with the derivatives of a Gaussian kernel $G_\sigma(s)$, being σ the standard deviation, according to the equations:

$$x'(s) = G'_\sigma(s) \otimes x(s), \quad x''(s) = G''_\sigma(s) \otimes x(s)$$
$$y'(s) = G'_\sigma(s) \otimes y(s), \quad y''(s) = G''_\sigma(s) \otimes y(s)$$

Gaussian-regularized derivatives were adopted to deal with ill-posedeness of differential operators [8]. In addition, the variability of the operator in contour tracing may introduce an additional source of noise. For these reasons, the value of σ was set to 8 pixel units (about 1.6 mm). Such a value ensured adequate regularization of differential operators without undesired smoothing effects. In Fig. 4 typical plots of $\kappa(s)$ are drawn for both the posteroanterior and the lateral views. The peaks due the diaphragmatic borders (B_{PA}, C_{PA} and B_{LL}, C_{LL} in posteroanterior and lateral projections, respectively) are quite evident in both cases.

The B_{PA} points and C_{PA} are utilized to segment the lung boundary (see Fig. 5). To this end, the apex A_{PA} is located as the boundary point farthest from the line segment $B_{PA}C_{PA}$. Afterward, the lung silhouette is split into three segments: left γ_{PA_1}, right γ_{PA_2}, and diaphragmatic γ_{PA_3} for the posteroanterior view. Similarly, for the lateral view, the points A_{LL}, B_{LL}, C_{LL} are similarly located and the posterior γ_{LL_1}, anterior γ_{LL_2}, and diaphragmatic γ_{LL_3} tracts are defined.

To describe the shape of each region in both the posteroanterior and the lateral, views, we computed the bending energy e_{γ_i} of the related curve segment γ_i:

$$e_{\gamma_i} = \int_{\gamma_i} \kappa(s)^2 \, ds, \quad i = 1, 2, 3$$

(for the sake of simplicity, the projection labels, PA and LL have been dropped). The bending energy is a classical

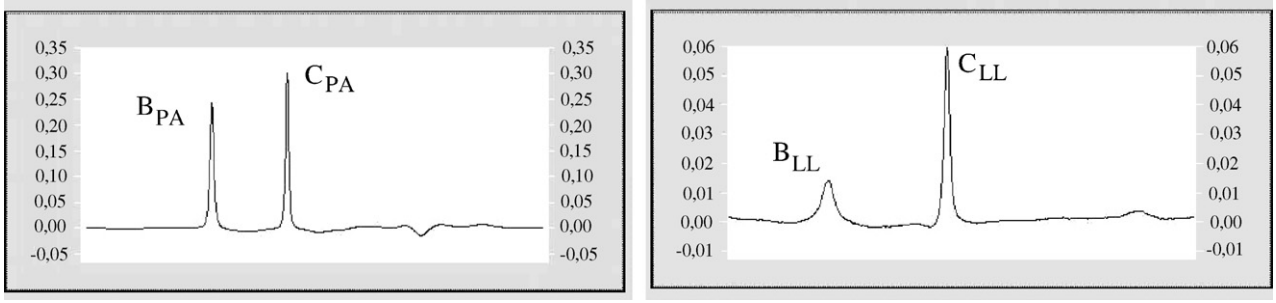

Fig. 4. The curvature of a typical lung boundary in the posteroanterior view is plotted in the left panel; B_{PA} and C_{PA} identify the diaphragmatic angles. Similarly, the curvature of a typical lung boundary in the lateral view is given in the right panel; B_{LL} and C_{LL} identify the diaphragmatic angles.

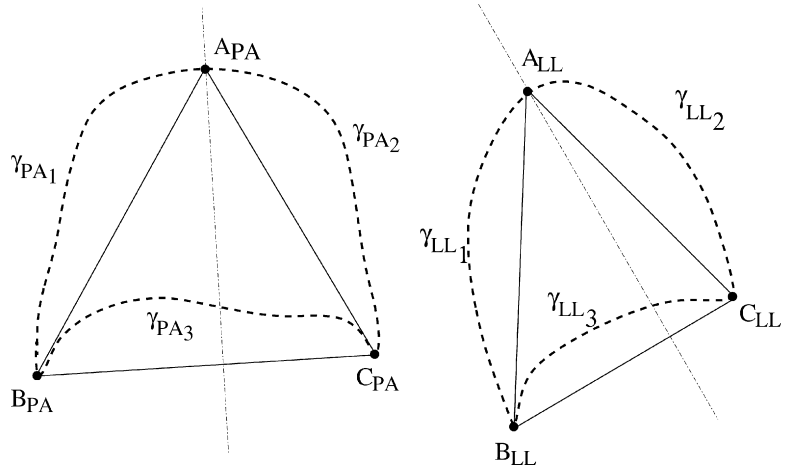

Fig. 5. Segmentation of the lung silhouette into anatomical regions in posteroanterior and lateral views.

measure of the curve deflection and has often been used to model biological shapes (see for example [9]). In the case of a straight line e_γ is null and it increases with the curve bending. Boundary changes in patient affected by emphysema should alter e_γ as compared to normal subjects.

In addition we estimated the amplitude of the angles α_1, α_2, and α_3 (see Fig. 6) which are prominent characteristics of the shape of the lung boundary: in the presence of emphysema one usually expects that the diaphragmatic angles be markedly widened (see Table 1). To summarize, for each radiographic projection we extracted a vector of six shape features:

$$\mathbf{f}_k = e_{\gamma_1}, e_{\gamma_2}, e_{\gamma_3}, \alpha_1, \alpha_2, \alpha_3$$

2.3.1.2. Minimal-polyline description. In a second approach to lung shape description we relied on the extraction of a discrete set of feature points. Given the nature of the problem at hand, one has mainly to capture alterations of the points that, in each anatomical segment, exhibit maximal bending properties.

To this end, starting from the three feature points (A, B, C) previously defined, we approximated the lung contour (in both views) with a six-point polyline.

In particular, we located three further key-points (P, Q, R) (see Fig. 7) by means of an algorithm based on the minimization of the maximum approximation error. Details of the algorithm are given in the Appendix A. The traced silhouette is thus replaced by the discrete point set (A, R, C, P, B, Q).

The shape of each segment of the lung boundary is therefore defined by the shape of one of the triangles:

$$T_1 = BQA, \quad T_2 = ARC, \quad T_3 = BPC$$

Consequently, alterations of the lung shape are referred to the changes of the shape of three triangles for each radiographic projection.

Each segment of the lung boundary is characterized by computing, in the corresponding triangle, the following

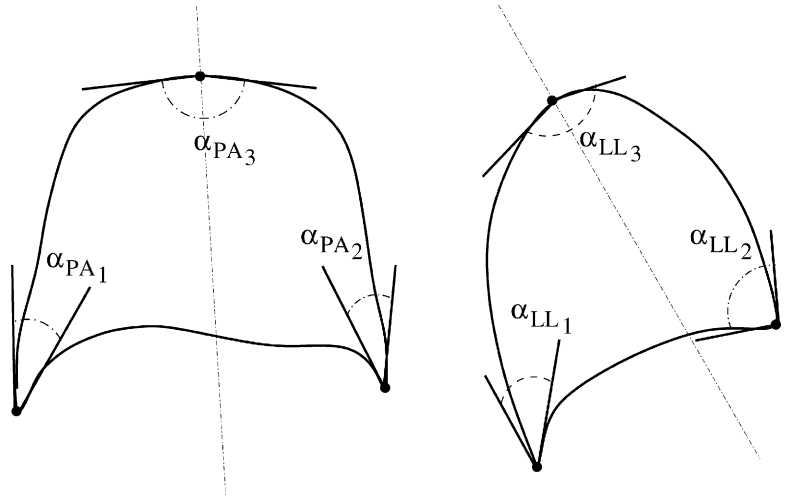

Fig. 6. Angular features in posteroanterior and lateral views.

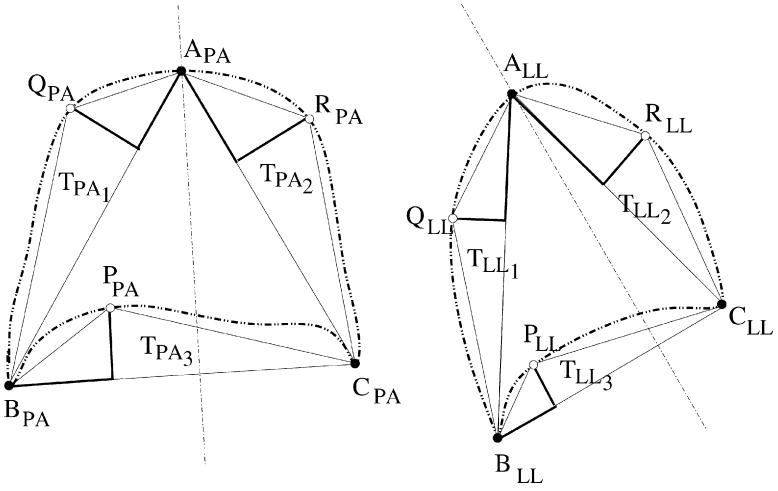

Fig. 7. Polyline approximation of lung silhouette in posteroanterior and lateral views.

numerical features:

$$\text{normalized area} : a_{i_n} = \frac{a_i}{a_{\text{LUNG}}}$$

$$\text{height ratio} : r_{i_{hb}} = \frac{h_i}{b_i}$$

$$\text{base ratio} : r_{i_{bb}} = \frac{b_{i_1}}{b_i}$$

where a_i is the area of the ith triangle, a_{LUNG} the area of the silhouette in the considered projection, h_i the height, b_i the length of the related base, b_{i_1} measures the projection on the basis of the triangle side nearest to the apex (right, left, anterior and posterior segments), or the leftmost point for the diaphragmatic segments (see Fig. 7). The normalized area (in all cases we have $0 < a_{i_n} < 1$) is a measure of the size of each triangle with respect to the overall lung-silhouette area. In emphysematous patients its value is expected to decrease in the diaphragmatic region whereas it may increase for the anterior segment in the lateral view, as well as in right and left segments in the posteroanterior one. The height–base ratio (in our cases $0 < r_i < 1$) estimates the amount of bending of each segment. It measures the zone of maximum bending of a given anatomical segment. The base ratio ($0 < r_i < 1$) gives the position where the maximum bending is reached with respect to base length. For each radiographic projection we extracted a vector of nine shape features:

$$\mathbf{f}_{\text{poly}} = a_{1_n}, a_{2_n}, a_{3_n}, r_{1_{hb}}, r_{2_{hb}}, r_{3_{hb}}, r_{1_{bb}}, r_{2_{bb}}, r_{3_{bb}}.$$

2.4. Neural network training and testing

To evaluate the discriminating power of the two previous feature sets, we studied the following classification tasks:

(C_1) recognition of emphysema patterns in the whole dataset;

(C_2) recognition of emphysema patterns in the sample of patients with COPD.

In both instances, we utilized the two sets of pattern vectors $\mathbf{f}_\kappa$, $\mathbf{f}_{\text{poly}}$ separately. Moreover, we tested the role of each projection by using (i) the parameters from both the posteroanterior and lateral views, (ii) the parameters from each single view separately.

To implement pattern recognition processes, we utilized multi-layer neural networks of the feed-forward type. It should be considered that, by using networks of adequate complexity, one is usually able to implement complex categorizations such as those that often occurs in medical diagnosis [10]. One advantage of such classifiers is that they can estimate the posterior probabilities required for Bayesian inference without the need for prior assumptions about the underlying probability distributions [10]. In addition, multilayer networks remain a popular neural classifier, which has been used successfully in a wide range of applications [11], including CAD systems in chest radiography [12,13].

Fig. 8 shows the typical configuration used here to solve both C_1 and C_2. All the hidden units have logistic sigmoid activation functions, whereas the output units have linear activation functions.

According to this scheme, several networks with different complexity were trained. As the activation functions were kept fixed, topology was the main factor affecting network complexity. Topology was varied according to: (a) the used set of shape features ($\mathbf{f}_\kappa$ or $\mathbf{f}_{\text{poly}}$), (b) the number of considered radiographic views, (c) the number of hidden layers, and (d) the number of units in each hidden layer. The number of input units is fixed by the feature set and the number of radiographic views used for the analysis. The curvature features $\mathbf{f}_\kappa$ imposes six units per each view, whereas nine units per view are needed when using $\mathbf{f}_{\text{poly}}$. As to the hidden layers, all the experiments were performed employing both one and two hidden layers each with a varying number of units. In

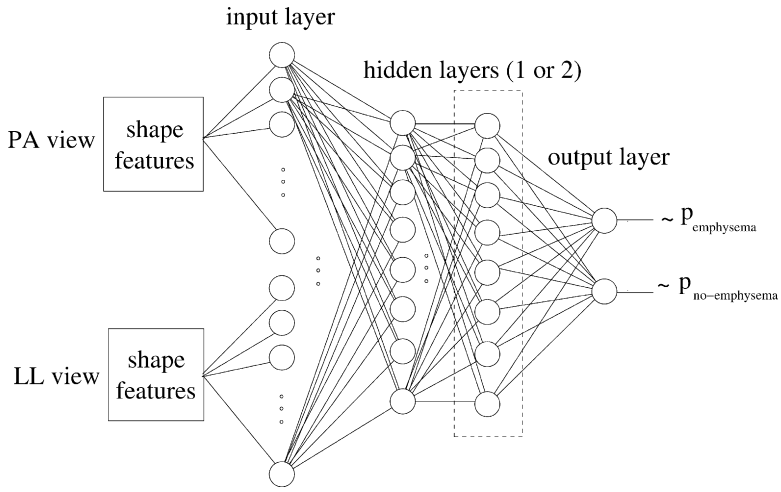

Fig. 8. Configuration of multilayer neural networks.The input shape featutheres can be either $\mathbf{f}_\kappa$ or $\mathbf{f}_{\text{poly}}$. Networks having both one or two hidden layers were considered. Each of two output units provides an estimate of the probability the input belongs to the classes "emphysema" and "no-emphysema", respectively.

both the classification problems C_1 and C_2, the input must be assigned either to the "emphysema" category or to the "no-emphysema" category. Consequently, two output units are used in all cases. The activation value of the first output unit estimates posterior probability of the input pattern belonging to the class "emphysema". Similarly, the second output unit approximates posterior probability of the input pattern belonging to the category "no-emphysema". This choice is the classical 1-of-c encoding ($c = 2$), the actual category of each input pattern is decided by looking at the output unit with the maximum activation [10]. In Table 2 we summarize the different topologies of the networks experimented in this work.

To train the networks we utilized a 10-fold cross-validation procedure. Cross-validation has the well-known advantage of using the entire dataset both in training and testing phases. In our case, the dataset was randomly split into 10 segments, each containing 16 normal subjects, 10 COPD patients, and 6 COPD patients with emphysema. In this way, for each experiment, we obtained 10 neural networks, each trained using 9 segments of the dataset and validated on the remaining data segment. Training of each single network was carried out minimizing the sum-of-squares error function. To this end error back-propagation using stochastic on-line weight update was employed [10]. To increase convergence rate, adaptive learning-rate (initial value 0.1) and momentum term (0.9) were included [10]. Moreover, to minimize the risk of being trapped in local minima, all the training procedures were repeated 10 times starting with different random initialization of networks weights. Only the best network, defined as the one providing the largest number of correct classifications, was retained. In any case, convergence of training was assumed to occur when the error on the test set begins to increase, or stabilizes. Training was carried out using a proprietary software running on a computer equipped with an AMD Athlon processor clocked at 2 GHz and 1 Gbyte RAM. The observed training time for a single network ranged from about 1×10^2 to 5×10^2 s, depending on network complexity. A complete cross-validation run took approximately from 1×10^4 to 5×10^4 s, as the network complexity increases.

Several parameters can be used to evaluate system performances. Among these we decided to adopt classification accuracy, sensitivity, and specificity that were defined as follows. Let P be the number of positive cases and N the number

Table 2
Summary of the network topologies adopted in our experiments

Experiment	Views	Feature-set	Input units	1st hidden layer	2nd hidden layer (when used)
C_1	Posteroanterior or lateral	$\mathbf{f}_\kappa$	6	3, 4, 5, 6, 7, 8, 9	3, 4, 5
		$\mathbf{f}_{\text{poly}}$	9	4, 5, 6, 7, 8, 9, 10	3, 4, 5, 6, 7, 8
	Posteroanterior and lateral	$\mathbf{f}_\kappa$	12	6, 7, 8, 9, 10	4, 5, 6, 7, 8
		$\mathbf{f}_{\text{poly}}$	18	8, 9, 10, 11, 12	4, 5, 6, 7, 8, 9, 10
C_2	Posteroanterior or lateral	$\mathbf{f}_\kappa$	6	3, 4, 5, 6, 7, 8, 9	3, 4, 5
		$\mathbf{f}_{\text{poly}}$	9	4, 5, 6, 7, 8, 9, 10	4, 5, 6, 7, 8
	Posteroanterior and lateral	$\mathbf{f}_\kappa$	12	6, 7, 8, 9, 10	6, 7, 8
		$\mathbf{f}_{\text{poly}}$	18	8, 9, 10, 11, 12	7, 8, 9, 10

In C_1 recognition of emphysema in all dataset is considered, in C_2 recognition of emphysema is done in the sample of patients with COPD.

of negative ones, for each of the 10 networks the quantities were computed:

$$\mathrm{TP} = \frac{\text{True positives}}{P}, \quad \mathrm{TN} = \frac{\text{True negatives}}{N}$$
$$\mathrm{FP} = \frac{\text{False positives}}{N}, \quad \mathrm{FN} = \frac{\text{False negatives}}{P}$$

The true positive rate, TP, and the true negative rate, TN, are the sensitivity and specificity, respectively. The accuracy, defined as the rate of correct classifications (CC), was computed by:

$$\mathrm{CC} = \frac{\text{True positives} + \text{True negatives}}{P + N}$$

The latter parameter may be sensitive to differences between the numbers of positives and negatives so that, for example, an increased specificity may affect CC more than an increased sensitivity. However, the availability of sensitivity and specificity values helps to overcome possible drawbacks of using accuracy alone.

The overall classification performances were estimated by averaging the performances of the 10 networks.

3. Results

3.1. Shape features

Table 3 shows the average values of the curvature-based parameters as computed in normals, patients with COPD and patients with COPD and emphysema, respectively. As indicated in the Table 3, the diaphragmatic angles, as measured in the posteroanterior and lateral views, were substantially wider in patients with COPD than in normal subjects. Conversely, no significant differences were found among the three groups, for what concerns the width of the apical angles. The bending energy values of the anatomical segments in the posteroanterior view showed a rather uniform decrease in COPD with respect to normals.

A different behaviour was observed in emphysema, right and left segments having a bending-energy value intermediate between normal subjects and COPD patients. Conversely the bending-energy of the diaphragmatic segments was the lowest in patients with emphysema. The energy parameters computed for the lateral view were lower in COPD patients as compared to normal subjects. The values for emphysema patients suggest that lateral views tend to be "more symmetric", being the bending energy of the anterior segment similar to that of the posterior segment. In addition, an increased bending of the anterior segment seems to be present on the average. As to the diaphragm segment a markedly reduced energy was observed.

Table 4 reports the average value of the parameters obtained for the minimal-polyline feature set. In the posteroanterior views, the normalized area a_n in COPD patients exhibited a slight increase in both the lateral segments, and a modest decrease in the diaphragmatic segment. A similar pattern was observed in the emphysema group which featured more evident changes. As to the lateral view, the normalized area of the diaphragmatic segments was remarkably smaller in patients with COPD, and even more in those with emphysema than in normal subjects.

The height ratio r_{hb} in the posteroanterior views showed a moderate increase in COPD patients, and this was more evident in emphysema patients. The r_{hb} parameter of diaphragmatic regions decreases in COPD patients and more conspicuously in emphysema patients. Values obtained in the lateral views confirmed observations made in the posteroanterior views—the diaphragmatic segment usually appearing very flattened in emphysema patients, and to a

Table 3
Curvature-based feature-set: data are means ± standard deviation

View	Patient group	α_1	α_2	α_3
Posteroanterior	Normals	31.62 ± 8.64	33.95 ± 8.66	166.30 ± 4.77
	COPD	38.70 ± 19.28	37.64 ± 12.92	160.76 ± 3.58
	Emphysema	46.94 ± 13.60	47.45 ± 16.42	162.13 ± 4.46
Lateral	Normals	49.78 ± 12.91	73.72 ± 19.59	140.60 ± 7.82
	COPD	55.34 ± 15.36	82.11 ± 17.80	140.66 ± 9.26
	Emphysema	69.91 ± 16.14	91.27 ± 24.51	142.13 ± 7.74

		Bending energy e_γ (μm^{-1})		
		e_{γ_1}	e_{γ_2}	e_{γ_3}
Posteroanterior	Normals	$5.81 \times 10^{-4} \pm 1.01 \times 10^{-4}$	$5.92 \times 10^{-4} \pm 1.21 \times 10^{-4}$	$6.63 \times 10^{-3} \pm 1.22 \times 10^{-4}$
	COPD	$5.48 \times 10^{-4} \pm 1.06 \times 10^{-4}$	$5.48 \times 10^{-4} \pm 1.12 \times 10^{-4}$	$4.61 \times 10^{-3} \pm 1.39 \times 10^{-4}$
	Emphysema	$5.68 \times 10^{-4} \pm 1.22 \times 10^{-4}$	$5.91 \times 10^{-4} \pm 1.43 \times 10^{-4}$	$2.01 \times 10^{-3} \pm 2.42 \times 10^{-4}$
Lateral	Normals	$6.20 \times 10^{-4} \pm 3.08 \times 10^{-4}$	$2.89 \times 10^{-4} \pm 1.23 \times 10^{-4}$	$5.33 \times 10^{-3} \pm 1.31 \times 10^{-4}$
	COPD	$5.07 \times 10^{-4} \pm 2.79 \times 10^{-4}$	$3.07 \times 10^{-4} \pm 1.00 \times 10^{-4}$	$4.49 \times 10^{-3} \pm 1.41 \times 10^{-4}$
	Emphysema	$3.25 \times 10^{-4} \pm 1.95 \times 10^{-4}$	$3.35 \times 10^{-4} \pm 8.24 \times 10^{-4}$	$1.97 \times 10^{-3} \pm 1.52 \times 10^{-4}$

In the top panel, α_1 and α_2 are the diaphragmatic angles, and α_3 is the apical angle (see also Fig. 6). In the bottom panel, e_{γ_1}, e_{γ_2} and e_{γ_3} are the bending energies of the related anatomical segments (see also Fig. 5).

Table 4
Polyline-based feature-set: data are means ± standard deviation

View	Patient group	T_1	T_2	T_3
Normalized area a_n				
Posteroanterior	Normals	0.221 ± 0.030	0.218 ± 0.032	0.194 ± 0.047
	COPD	0.225 ± 0.036	0.227 ± 0.035	0.174 ± 0.056
	Emphysema	0.236 ± 0.031	0.232 ± 0.037	0.131 ± 0.047
Lateral	Normals	0.223 ± 0.030	0.213 ± 0.032	0.132 ± 0.051
	COPD	0.240 ± 0.030	0.254 ± 0.029	0.095 ± 0.060
	Emphysema	0.250 ± 0.031	0.265 ± 0.032	0.050 ± 0.051
Height ratio r_{hb}				
Posteroanterior	Normals	0.219 ± 0.023	0.220 ± 0.030	0.148 ± 0.033
	COPD	0.223 ± 0.031	0.224 ± 0.030	0.132 ± 0.047
	Emphysema	0.245 ± 0.030	0.247 ± 0.034	0.123 ± 0.044
Lateral	Normals	0.261 ± 0.052	0.265 ± 0.061	0.165 ± 0.062
	COPD	0.272 ± 0.058	0.285 ± 0.056	0.097 ± 0.074
	Emphysema	0.322 ± 0.082	0.334 ± 0.071	0.051 ± 0.021
Base ratio r_{bb}				
Posteroanterior	Normals	0.464 ± 0.022	0.481 ± 0.026	0.375 ± 0.019
	COPD	0.448 ± 0.024	0.474 ± 0.028	0.360 ± 0.024
	Emphysema	0.481 ± 0.020	0.482 ± 0.026	0.520 ± 0.021
Lateral	Normals	0.221 ± 0.033	0.181 ± 0.025	0.486 ± 0.038
	COPD	0.219 ± 0.027	0.172 ± 0.023	0.491 ± 0.033
	Emphysema	0.182 ± 0.021	0.157 ± 0.022	0.505 ± 0.032

The values of normalized area, height ratio and base ratio are given for each of the triangles T_1, T_2 and T_3 representing the lung silhouette (see also Fig. 7).

minor extent in COPD patients. Values of base ratio r_{bb} suggest that, in emphysematous patients, maximum bendings of right and left segments (in the posteroanterior view) and anterior and posterior segments (in the lateral view) tend to move towards upper locations. In the diaphragmatic segments such a maximum bending seems to be placed at about the center of the segments itself.

3.2. Recognition of emphysema patterns

Discrimination accuracy of emphysematous patients (termed Positives, 60 cases) from all the other cases (Negatives, 260 cases) is given in Table 5, for the two feature-sets $\mathbf{f}_\kappa$ and $\mathbf{f}_{\text{poly}}$ using both the posteroanterior and lateral views. The number of units per layer of the related neural network is also given. By using $\mathbf{f}_\kappa$, 249 ± 13.5 cases were correctly classified (43 ± 3.1 true positives and 206 ± 10.1 true negatives). For the $\mathbf{f}_{\text{poly}}$ set, correct classifications were 289 ± 4.1 (53 ± 1.2 true positives and 236 ± 2.4 true negatives).

Table 5
Detection of emphysema in the entire dataset using both the posteroanterior and lateral projections

Feature-set	CC (%)	TP (%)	TN (%)	FN (%)	FP (%)	NN units per layers
$\mathbf{f}_\kappa$	77.8	71.7	79.2	28.3	20.8	12-6-6-2
$\mathbf{f}_{\text{poly}}$	90.3	88.3	90.7	11.7	9.3	18-8-6-2

The correct classification rate (CC) is given along with the true positive (TP), true negative (TN), false negative, and false positive rates, respectively. The number of units per layer of the related neural network (NN) is in the rightmost column.

Table 6
Detection of emphysema in the entire dataset using the posteroanterior projection alone

Feature-set	CC (%)	TP (%)	TN (%)	FN (%)	FP (%)	NN units per layer
$\mathbf{f}_\kappa$	72.2	68.3	73.1	31.7	25.0	6-8-2
$\mathbf{f}_{\text{poly}}$	80.3	76.7	86.1	23.3	18.8	9-6-5-2

Labels are the same as in Table 5.

In order to evaluate the importance of each single projection in the recognition task, we trained a different set of neural networks by using either the posteroanterior or the lateral projections separately. The results obtained are given in Tables 6 and 7, respectively. In particular, by using $\mathbf{f}_\kappa$ from the posteroanterior view alone, 231 ± 15.2 cases were correctly classified (41 ± 4.2 true positives and 190 ± 12.2 true negatives). For the $\mathbf{f}_{\text{poly}}$ set computed in the same view, 257 ± 7.4 correct classifications were obtained (46 ± 3.3 true positives and 211 ± 10.7 true negatives). With the lateral view alone, we had a number of correct assignments of 241 ± 13.7 (42 ± 3.2 true positives and 199 ± 11.1 true negatives) by using $\mathbf{f}_\kappa$. For the $\mathbf{f}_{\text{poly}}$ set computed in the same

Table 7
Detection of emphysema in the entire dataset using the lateral projection alone

Feature-set	CC (%)	TP (%)	TN (%)	FN (%)	FP (%)	NN units per layer
$\mathbf{f}_\kappa$	75.3	70.7	74.4	26.3	25.6	6-8-2
$\mathbf{f}_{\text{poly}}$	81.9	83.3	81.5	16.7	18.5	9-6-5-2

Labels are the same as in Table 5.

Table 8
Detection of radiological emphysema in COPD patients using both the posteroanterior and lateral projections

Feature-set	CC (%)	TP (%)	TN (%)	FN (%)	FP (%)	NN units per layer
$\mathbf{f}_\kappa$	81.9	76.7	85.0	23.3	15.0	12-8-4-2
$\mathbf{f}_{\text{poly}}$	90.6	90.0	91.0	10.0	9.0	18-8-4-2

Labels are the same as in Table 5.

Table 9
Detection of radiological emphysema in COPD patients using the posteroanterior projection

Feature-set	CC (%)	TP (%)	TN (%)	FN (%)	FP (%)	NN units per layer
$\mathbf{f}_\kappa$	73.4	71.6	79.0	28.3	21.0	6-4-2
$\mathbf{f}_{\text{poly}}$	81.2	80.0	82.0	20.0	18.0	9-6-3-2

Labels are the same as in Table 5.

view, 262 ± 6.2 cases were correctly classified (50 ± 2.1 true positives and 212 ± 3.1 true negatives).

The classification performances for both feature sets ($\mathbf{f}_\kappa$ and $\mathbf{f}_{\text{poly}}$) in recognising emphysema within the group of patients with COPD (160 cases) are reported in Table 8. By using $\mathbf{f}_\kappa$, a number of 131 ± 6.1 correct classification was obtained (46 ± 1.5 true positives and 85 ± 4.2 true negatives). For the $\mathbf{f}_{\text{poly}}$ set, 145 ± 5.0 cases were correctly classified (54 ± 1.0 true positives and 91 ± 4.4 true negatives).

Results obtained by employing either the posteroanterior or the lateral views alone are given in Tables 9 and 10, respectively. As to the posteroanterior view, the feature-set $\mathbf{f}_\kappa$ yielded 122 ± 6.8 correct classifications (43 ± 2.3 true positives and 79 ± 4.2 true negatives). For the $\mathbf{f}_{\text{poly}}$ set computed in the same view, 130 ± 5.6 cases were correctly classified (48 ± 2.8 true positives and 82 ± 3.9 true negatives). In the case of the lateral view alone, by using $\mathbf{f}_\kappa$, 128 ± 6.5 cases were correctly assigned to the related classes (45 ± 2.0 true positives and 83 ± 4.3 true negatives). For the $\mathbf{f}_{\text{poly}}$ set computed in the same view, 136 ± 5.1 cases resulted correctly classified (50 ± 1.8 true positives and 86 ± 3.2 true negatives).

To conclude this section, we would like to aware the reader that also the combined use of the two feature sets $\mathbf{f}_\kappa$ and $\mathbf{f}_{\text{poly}}$ was analyzed. As previously described for the case of a single feature set, we studied: the two classification problems C_1 (recognition of emphysema in the entire dataset) and C_2 (recognition of emphysema in COPD patients); the use of single or two-sided view, and the effects of ANN complexity. Results parallel those obtained by using $\mathbf{f}_{\text{poly}}$ alone and therefore are not reported. Seemingly, curvature features do not add significant information to polyline features.

Table 10
Detection of radiological emphysema in COPD patients using the lateral projection

Feature-set	CC (%)	TP (%)	TN (%)	FN (%)	FP (%)	NN units per layer
$\mathbf{f}_\kappa$	80.0	75.0	83.0	25.0	17.0	6-6-2
$\mathbf{f}_{\text{poly}}$	85.6	83.3	86.0	16.7	19.4	9-6-4-2

Labels are the same as in Table 5.

4. Discussion and conclusion

The results of our study support that pulmonary emphysema can be reliably diagnosed or excluded by using digital chest radiographs and a proper computational aid. Actually, lung contours can be reliably traced by using a small set of knot points that can be clearly identified in the imaged anatomy. Moreover, the adopted analysis of the shape of the lung silhouette exhibits a high discriminant power adequate to assess emphysema in a dataset including COPD patients and subjects with normal lung function tests.

Data shown in previous section suggest several considerations. First of all, the use of an adequate computational description is crucial. Even though values computed for $\mathbf{f}_\kappa$ and $\mathbf{f}_{\text{poly}}$ (see Section 3) suggest that both feature-sets were sensitive to emphysema-related abnormalities, classification results based on minimal-polyline features $\mathbf{f}_{\text{poly}}$ were significantly better than those obtained from curvature-based features $\mathbf{f}_\kappa$. As to the detection of emphysema in the entire dataset using both the posteroanterior and lateral projections, the polyline method provided an overall accuracy of about 90%, with 88% sensitivity and 90% specificity. When using curvature method, accuracy was about 77% with sensitivity less than 72% and specificity about 79%. Classification based on single projections exhibited a significant performance degradation for both methods as compared to two-sided-based description. Accuracy decreased to about to 72% (sensitivity less than 69%, specificity 73%) using $\mathbf{f}_\kappa$ computed from posteroanterior radiograms, and to about 80% (sensitivity 77% and specificity 86%) using $\mathbf{f}_{\text{poly}}$. In the case of the lateral projection, for $\mathbf{f}_\kappa$ the accuracy was 80% (sensitivity 75%, specificity 83%), while for $\mathbf{f}_{\text{poly}}$ it was of about 85% (sensitivity 83.3%, specificity 86%). It is worth mentioning that $\mathbf{f}_{\text{poly}}$ always yielded better results than $\mathbf{f}_\kappa$, and that the analysis based on the lateral view alone was more accurate than that based on the posteroanterior view alone. A reasonable explanation of the latter finding is that the lateral view provides a clear visualization of the retrosternal space that is usually widened in patients with emphysema. Although neither $\mathbf{f}_\kappa$ or $\mathbf{f}_{\text{poly}}$ feature-sets provide direct measurement of the width of the retrosternal space, nonetheless widening of the retrosternal space due to emphysema results in morphological alterations (protrusion) of the anterior segment of the lung silhouette. Proper shape features can capture such abnormalities. Above considerations apply to the evaluation of the emphysema in the group of patients with COPD.

In the present study, the diagnosis or exclusion of emphysema was based on four explicit radiologic criteria that were validated against lung pathology [3]. Even though these criteria turned out to be very accurate, it is likely that mild emphysema may, in some instances, go undetected on chest radiographs. Therefore, it would be appropriate

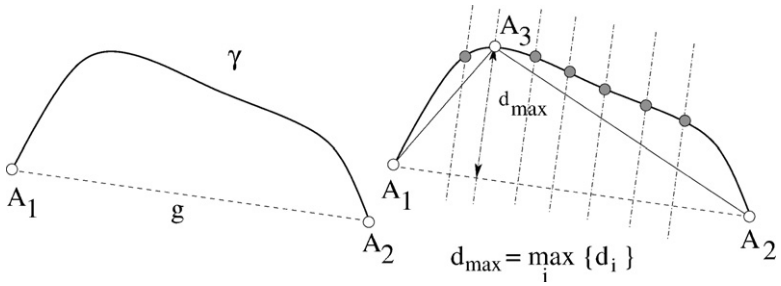

Fig. 9. Computation of approximating polyline.

to further validate the computational descriptors described here in a new sample of patients using high-resolution computed tomography as reference diagnostic standard for emphysema. In summary, computational descriptors of lung shape, as derived from digital chest radiographs, are able to detect emphysema with high degree of accuracy. Two-sided chest radiographs provide more accurate discrimination than single-view analysis. Moreover, neural network classifiers allow the implementation of complex decision processes and appear well suited to face the considered task.

Appendix A

The approximating polyline of the lung contour γ was computed by the following recursive algorithm [14]. Let A_1 and A_2 be the starting and ending point, respectively, of the curve γ, and A_i the intermediate points (see Fig. 9), then:

(1) Draw the straight line through A_1 and A_2 and assume it a approximating polyline g.
(2) For each point A_i of the curve compute the distance d_i from g.
(3) Pick the curve point farthest from g and assume it as a new feature point, replace the segment of with two line segments.
(4) Recursively apply the algorithm until the desired number of points is reached (or some other stopping criterion is met).

In the case considered, we approximated each segment of the lung boundary by a three points polyline. One can look at initial straight line as a zeroth-order approximation of the curve. In this view, we used a first-order approximation. Though a more accurate curve representation could be utilized by adding further key-points, the adopted scheme was adequate for the problem at hand, being able to capture both the size of each boundary segment, its maximal bending and the position where such a bending is reached.

References

[1] Ciba Guest Symposium Report. Terminology, definitions, and classification of chronic pulmonary emphysema and related conditions. Thorax 1959;14:286–99.
[2] Thurlbeck WM, Müller NL. Emphysema: definition, imaging, and quantification. Am J Roentgenol 1994;163:1017–25.
[3] Sutinen S, Christoforidis AJ, Klugh GA, Pratt PC. Roentgeno-logic criteria for the recognition of nonsymptomatic pulmonary emphysema, correlation between roentgenologic findings and pulmonary pathology. Am Rev Respir Dis 1965;91:69–76.
[4] Pratt PC. Role of conventional chest radiography in diagnosis and exclusion of emphysema. Am J Med 1987;82:998–1006.
[5] Schaefer-Prokop C. Plain chest radiography: the digital revolution. Eur Respir Mon 2004;30:23–38.
[6] van Ginneken B, ter Haar Romeny BM, Viergever M. Computer-aided diagnosis in chest radiography: a survey. IEEE Trans Med Imaging 2001;20:1228–41.
[7] Chappell S, Daly L, Morgan K, Guetta-Baranes T, Roca J, Rabinovich R, et al. Cryptic haplotypes of SERPINA1 confer susceptibility to chronic obstructive pulmonary disease. Hum Mutat 2006;27:103–9.
[8] Worring M, Smeulders AWM. Digital curvature estimation. CVGIP: Image Understanding 1993;58:366–82.
[9] Duncan JS, Lee F, Smeulders A, Zaret BL. A bending energy model for measurement of cardiac shape deformity. IEEE Trans Med Imaging 1991;10:307–20.
[10] Bishop CM. Neural networks for pattern recognition. Oxford University Press; 1995.
[11] Cohen ME, Hudson DL. Neural networks artificial intelligence for biomedical engineering. New York: Wiley-IEEE Press; 1999.
[12] Lo S-CB, Lou S-LA, Lin J-S, Freedman M, Chien MV, Mun SK. Artificial convolutional neural networks techniques and applications for lung nodule detection. IEEE Trans Med Imaging 1995;14:711–8.
[13] Coppini G, Diciotti S, Falchini M, Villari N, Valli G. Neural networks for computer-aided diagnosis: detection of lung nodules in chest radiograms. IEEE Trans Inf Technol Med 2003;7:344–57.
[14] Duda RO, Hart PE. Pattern recognition and scene analysis. New York: Wiley; 1973.